computers

MDPI

Article

Model Structure Optimization for Fuel Cell Polarization Curves

Markku Ohenoja *, Aki Sorsa and Kauko Leiviskä

Control Engineering, University of Oulu, P.O. Box 4300, FI-90014 Oulu, Finland; aki.sorsa@oulu.fi (A.S.); kauko.leiviska@oulu.fi (K.L.)

* Correspondence: markku.ohenoja@oulu.fi; Tel.: +358-29-448-2473

Received: 4 September 2018; Accepted: 6 November 2018; Published: 9 November 2018

Abstract: The applications of evolutionary optimizers such as genetic algorithms, differential evolution, and various swarm optimizers to the parameter estimation of the fuel cell polarization curve models have increased. This study takes a novel approach on utilizing evolutionary optimization in fuel cell modeling. Model structure identification is performed with genetic algorithms in order to determine an optimized representation of a polarization curve model with linear model parameters. The optimization is repeated with a different set of input variables and varying model complexity. The resulted model can successfully be generalized for different fuel cells and varying operating conditions, and therefore be readily applicable to fuel cell system simulations.

Keywords: model identification; genetic algorithms; fuel cell

1. Introduction

Hydrogen-fed polymer electrolyte membrane fuel cells (PEMFC) are known to be an efficient and flexible energy conversion technique with the capability of operating in future carbon-free, renewable, and distributed energy markets. Although PEMFCs are already commercialized, further research, especially regarding stack level, is required [1]. Computational tools and numerical modeling of PEMFC stacks play an important role in studying the effect of operating conditions, system parameters, and different configurations on fuel cell performance [2]. The fuel cell system comprises not only the fuel cell assembly, but also the auxiliary equipment related to fuel storage, air and fuel supply, cooling, and power conditioning [1]. In fuel cell stack models, electrochemical phenomena, energy balance, and mass balances are typically treated as separate modules. The electrochemical behavior of PEMFC is governed by the membrane electrode assembly, which is depicted in Figure 1, and characterized by a polarization curve, which is presented in Figure 2. An equivalent circuit model is used to determine the polarization curve of the fuel cell (FC) in the steady state. The dynamics of a FC are governed by the energy and mass balance, as well as their interlinkage to the polarization curve model.

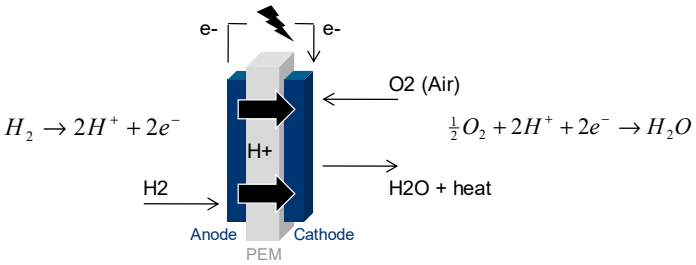

Figure 1. Membrane electrode assembly of a polymer electrolyte membrane fuel cell (PEMFC).

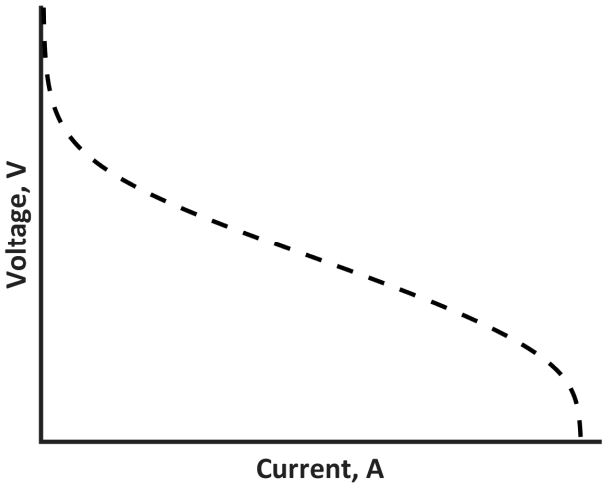

Figure 2. A typical PEMFC polarization curve.

The polarization curve depicts the voltage–current characteristics of a fuel cell. Typically, such a model is constructed to describe the thermodynamic potential (or the open-circuit voltage) and the different losses (or overvoltage) in the performance. Often, the model is presented as a parameterized semi-empirical model with a theoretical background [3–6]. In addition, several other model structures can be found in the literature, and they have been recently presented [7]. This kind of modeling approach aims to provide a generalizable model structure for different fuel cells, but it is simple enough to be utilized in a simulation of complete fuel cell power systems, where rigorous first principle (mechanistic) models may often be too complicated to be applied [2]. The semi-empirical models can also be found as a part of more rigorous fuel cell models [8].

Parameter estimation (or identification) of the above-mentioned semi-empirical models has gained a lot of attention over the past 10 years. In particular, it leads to an industrially relevant nonlinear optimization problem for evolutionary optimizers. Evolutionary optimizers are understood as heuristic search methods that mimic the evolution in nature. For example, established methods such as genetic algorithms [9,10], differential evolution [11,12], and many new methods [13–15] have been proven to work for the parameter estimation problem of the fuel cell polarization curve. During the course, the authors have also altered the model structure [15] in order to improve the model accuracy.

In this study, an alternative way of applying evolutionary optimizer tools for polarization curve modeling is presented. Our novel approach involves model structure identification for the steady-state FC polarization curve model. Although evolutionary optimizers, such as genetic programming [16], have previously been applied for determining solid oxide fuel cell models, they have been focused on reproducing the behavior of one FC system. Here, the aim is to find one model structure that can also be generalized to different PEMFC systems. The resulted FC polarization curve model is linear with respect to its parameters, but nonlinear by its variables. This significantly simplifies the parameter estimation part of the model development. Although the structure identification essentially leads to a data-driven black-box model, the models developed in this study can be considered semi-empirical or gray box, as they utilize some of the auxiliary equations that are used also in the well-known semi-empirical model [9,10,12]. In this study, the structure search results from Ohenoja et al. [7] are extended to handle an alternative input variable set, and the structure search is repeated with varying model complexity. The proposed model structure is validated for different fuel cells and operating conditions, and the applicability of the model is discussed.

The outlook of this paper is as follows. In Section 2, the optimization algorithm and the data utilized are presented. In Section 3, the model structure identification results for three different cases are presented. In Sections 4 and 5, the results are discussed, and the findings are summarized.

2. Materials and Methods

2.1. Fuel Cell Data

The fuel cell data used in this study originated from a visual interpretation of the polarization curve data in Mo et al. [9] and Xue et al. [17]. It comprises four different fuel cells, namely the SR-12, BCS, Ballard, and 250W. For the SR-12, BCS, and Ballard, 10 current–voltage pairs recorded in constant operating conditions are available [17]. For the 250W, the data sets consist of four polarization curves observed in different operating conditions, with each data set having 15 current–voltage pairs [9]. Hence, the fuel cell data comprises seven subsets, and the total number of current–voltage pairs, n_k, is 90.

In addition to current–voltage values, the FC operating conditions (temperature T, total pressure P_{tot}, anode pressure P_a, and cathode pressure P_c) can be used as input data for the model identification. This data was also available in [9,17], and it has further been complemented with the calculated values for the saturation pressure of water (p^{sat}_{H2O}), partial pressures of oxygen (p_{O2}) and hydrogen (p_{H2}), and anode oxygen concentration (C_{O2}). The equations adopted from Mo et al. [9] are presented in Appendix A. For the 250W FC, both anode and cathode relative humidity (RH_a and RH_c, respectively) are equal to one [9].

Also, the cell properties, such as the cell active area (A), membrane thickness (L_{mem}), resistivity of the membrane (ρ_{m}), limiting current (i_{lim}), and thermodynamic potential (E_0) can be utilized in the model development. The fuel cell data that was used in this study can be found in the Supplementary Material. In total, the data comprises one output, the FC voltage ($y(k)$), and nine possible input variable candidates $X_j(k)$, where k is an integer number between 1 and n_k, and j is an integer number between one and nine. The input data naturally comprise the FC current (i) and the limiting current in order to be able to model the FC voltage throughout the current range. The operating conditions (T, C_{O2}, p_{O2}, p_{H2}) and cell properties (L_{mem}, A) are needed to capture the voltage–current characteristics in different FC systems or in the different conditions of a single FC.

2.2. Reported Model Structures

Different kinds of model structures have been proposed to ensure the adequate prediction abilities of the polarization curve models. In Table 1, some of them are presented in terms of utilized variables and the number of free model parameters (n_p). It can be observed that the reported model structures are with varying complexity. A more detailed review is given in Ohenoja et al. [7]. As mentioned, these parameterized models are simplifications of electrochemical phenomena, and are easily tuned with the measurable variables from the operating fuel cells. With the aid of experimental data, the curve-fitting properties—and therefore the prediction abilities of the models—are further enhanced, but with the expense of losing the generalization abilities for the unseen FC systems. Purely empirical, or data-driven models for the FC polarization curve also exist [18], but they are not in the scope of this work.

Table 1. Overview on seven different polarization curve models showing the number of free parameters (n_p) and variables utilized (denoted by x in the table).

Ref.	n_p	i	P_{tot}	p_{O2}	i_{lim}	C_{O2}	T	p_{H2}	RH_a	RH_c	p^{sat}_{H2O}	P_a	P_c	A	L_m	ρ_{m}	E_0
[19]	2	x															x
[20]	3	x															x
[2]	5	x	x	x													x
[21]	4	x			x												x
[6]	10	x		x		x	x	x	x	x	x	x	x	x			x
[3]	6	x		x		x	x	x	x	x	x	x	x	x	x	x	x
[22]	7	x		x	x	x	x	x	x	x	x	x	x	x	x	x	x

2.3. Algorithm for Model Structure Identification

In this study, a generic model structure shared by all of the studied FCs is identified. The differences in voltage–current characteristics of the studied FCs are captured by their model parameters. Hence, model parameter estimation is performed separately for each FC. Finally, the model identification involves an internal validation step for one FC in different operating conditions. The overall approach is illustrated in Figure 3. The selected optimization method, encoding procedure, parameter estimation method, and performance evaluation strategy are described in the following subsections.

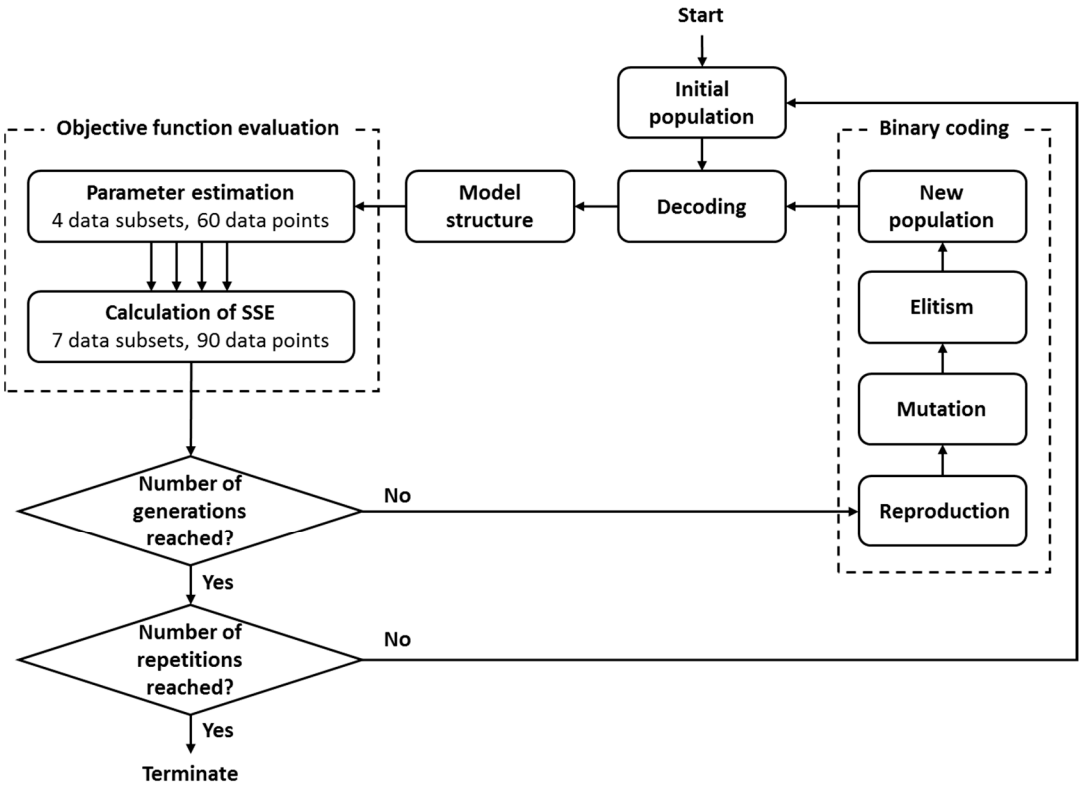

Figure 3. Identification algorithm.

2.3.1. Genetic Algorithms

A genetic algorithm (GA) is an optimization method mimicking evolution [23]. In this study, binary coded genetic algorithms are utilized to find an optimized nonlinear model structure. The coding and optimization are performed with Matlab® software. The genetic algorithm applied uses uniform crossover and mutation operations; tournament selection is used with the number of candidates set to five, and elitism is applied by replacing the worst candidate from the new generation with the best candidate from the previous generation. In all of the studied scenarios, the population size is 500, the number of generations is 100, the crossing probability is 0.9, the mutation probability is 0.05, and the optimization loop is repeated 100 times with different initial populations. The Matlab® random number generator was initialized prior to the execution in order to be able to repeat the results. The elitism ensures that the best individual is preserved throughout the generations in a single GA run. The overall best solution is selected among the 100 best individuals from GA repetitions. The GA objective function (fitness function) that was used is given in Section 2.3.4. As the optimization task in this study is not critical with respect to computational time, the selection of optimization algorithm tuning parameters is more guided by experience and an algorithms' ability to converge, rather than finding a compromise between convergence properties and computational time.

2.3.2. Chromosome Encoding and Decoding

The model structure identification comprises the selection of model variables, or features, mathematical operators for the selected features, and the arithmetic operations between the generated terms. In Figure 4, the chromosome encoding principle is presented. First, N_j bits are reserved to represent the different model variable candidates in the binary format. Similarly, the number of mathematical transformation operators (m) and uniting mathematical operators (u) to be tested are defined, and a correct number of bits (N_m and N_u) are determined, respectively. Finally, the allowable maximum number of variables (n) in the final model structure is defined, and the chromosome size is propagated to be able to describe the model structure in binary format. An example of binary coded chromosome with $j = 8$, $m = 4$, $u = 2$, $n = 3$ and the resulted mathematical expression after decoding are presented in Figure 5.

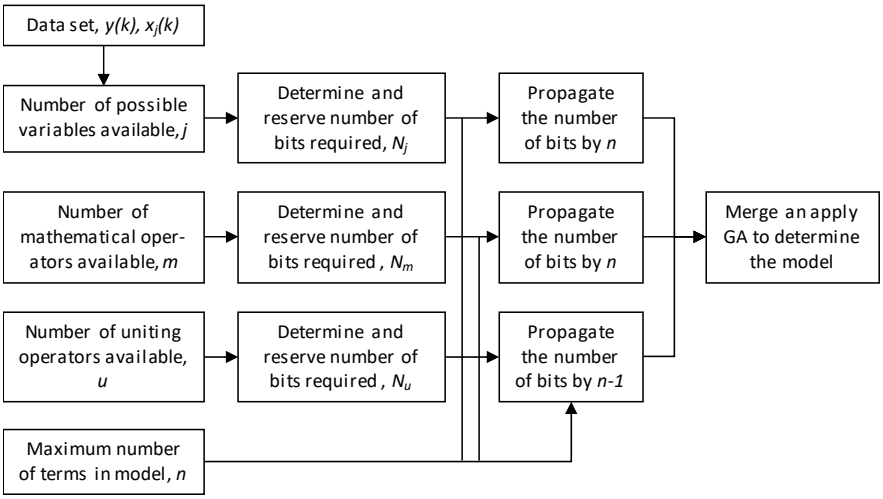

Figure 4. Encoding procedure.

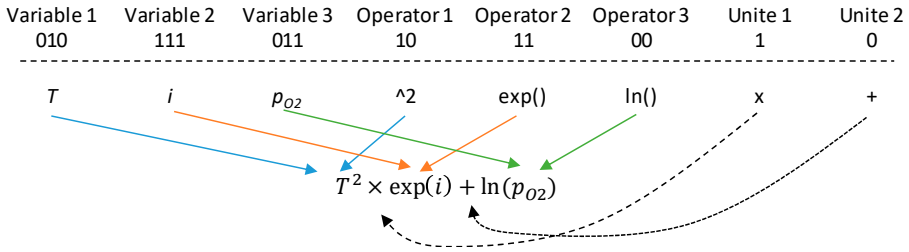

Figure 5. Example of binary coded chromosome and resulted mathematical expression for a three-term model structure ($n = 3$) with up to eight possible variables ($j = 8 = 2^3$, $N_j = 3$), four possible transformation operators ($m = 4 = 2^2$, $N_m = 2$), and two possible uniting operators ($u = 2 = 2^1$, $N_u = 1$).

The decoding is executed with a sequential approach by reading the chromosome bits determining the variable, the transformation operator, and the uniting operator. The result is collected to a matrix by calculating the first model term (T^2 in Figure 5) and adding a matrix column for it. Then, other model terms are dynamically added either as new columns (summation) or uniting the last matrix column with the new model term (multiplicative and power terms). Finally, a unit vector is added as a last column. The resulted matrix has a size of n_k rows and n_t columns, where $n_t \leq n + 1$.

The maximum number of model variable candidates was restricted to eight in this study, resulting as $N_j = 3$. Eight functional transformations (mathematical operators) are applied; 1, ^2, ^3, sqrt, exp(−), 1/, exp, and ln. Hence, three bits are required to describe these eight operations. The uniting mathematical operators that are used in this study are $+$, $\times$, $\div$, $\wedge$. These four operators are described

with two bits. The resulting individual contains a vector of bits, which are interpreted (decoded) into a model with the following general structure:

$$\hat{y}(k) = a_0 + a_1 f_1(+/\times/\div/\wedge)a_2 f_2(+/\times/\div/\wedge)...a_n f_n \quad (1)$$

where $\hat{y}(k)$ is the predicted FC voltage, $f_1 \ldots f_n$ are the selected variables among X_j with their mathematical transformations, and $a_0 \ldots a_n$ are the regression coefficients. Mathematical operators applied to the model variables may make the model nonlinear. The model can be solved as an ordinary regression equation, because it is always linear with respect to the regression coefficients. Since the terms are fused together, the number of regression coefficients (n_t) in the final model may also be less than the number of selected variables (n). However, this depends on the applied mathematical operators.

2.3.3. Parameter Estimation

GA provides the candidate solution for the model structure. The performance of that candidate is evaluated after the estimation of the regression coefficients. The parameter estimation problem is linear, and the least squares solution of Equation (2) gives the regression coefficients:

$$\begin{bmatrix} a_0 \\ \vdots \\ a_{nt-1} \end{bmatrix} = \begin{bmatrix} 1 & f_1(1) & \ldots & f_{nt-1}(1) \\ \vdots & \vdots & \ddots & \vdots \\ 1 & f_1(k) & \ldots & f_{nt-1}(k) \end{bmatrix}^{-1} \begin{bmatrix} y(1) \\ \vdots \\ y(k) \end{bmatrix} \quad (2)$$

where $y(k)$ is the measured FC voltage for n_k instances. As the inverted matrix is non-square, the Moore–Penrose pseudoinverse is used ('pinv' in Matlab®). Linear regression parameters are calculated separately for each cell. The data sets from SR-12, BCS, and Ballard, and the two data sets from 250W are utilized in the parameter estimation.

2.3.4. Objective Function and Model Performance

The model performance is evaluated based on the objective function value. The objective function utilized is the sum of squared errors (SSE) between the experimental voltage and the predicted voltage from the candidate model comprising all the available FC data sets:

$$SSE = \sum_{k=1}^{n_k} (y(k) - \hat{y}(k))^2 \quad (3)$$

As indicated in Figure 3, the parameter estimation utilizes 60 voltage–current pairs comprising the SR-12, BCS, and Ballard FC, and data sets 1 and 2 for the 250W FC. The objective function calculation incorporates all 90 available voltage–current pairs. The predicted values for data sets 3 and 4 for 250W FC are calculated based on the candidate solution for the model structure and the regression coefficients estimated with data sets 1 and 2. Overall, the optimized solution has a generalization ability with respect to different FCs; the model structure that was found can be used to represent four different FCs, when the FC specific model parameters are used. The data division also leads to a generalization ability with respect to different operating conditions; the 250W FC has four data sets, where only half of the data is utilized in parameter estimation, and the other half is used in an internal validation stage with the defined model structure and model parameters.

3. Results

The model structure identification is presented for three different cases. The model structure inspected in numerous studies [9,10,12,22] consists of seven unknown parameters. Hence, the first case presented in this study considers a maximum number of seven terms (n = 7) in the model structure,

ensuring a comparable model complexity with the widely used semi-empirical model structure. This case was also presented in Ohenoja et al. [7], and is here accompanied by new results from two additional cases. In the second case, a different set of possible model variable candidates is taken. In the third and final example, the model structure identification is performed with varying model complexity. The model structures presented are tested with four different FCs, one of them comprising polarization curves in four different operating conditions. The optimizations were run with 3.4 GHz, 12 GB i7 PC using Matlab® R2016a without parallel computing. The model structure search involved 5,000,000 objective function evaluations (and 20,000,000 regressions), requiring 38−51 min of wall-clock time, where the elapsed time increased linearly as a function of allowed model complexity.

3.1. Case 1

The input variables for the first case, which were also presented in [7], were i, T, C_{O2}, p_{O2}, p_{H2}, i_{lim}, and a calculated variable, i/i_{lim}. The optimization results for the nominal model complexity are presented in Figure 6, where the seven predicted polarization curves with experimental data are shown. Clearly, the model can follow the experimental data very accurately. In Table 2, the *SSE* values for each case are given. In comparison, the *SSE* values from our earlier studies [10,24] are given. It should be noted that all of these studies use exactly the same data sets, and thus, a comparison of *SSE* values is straightforward.

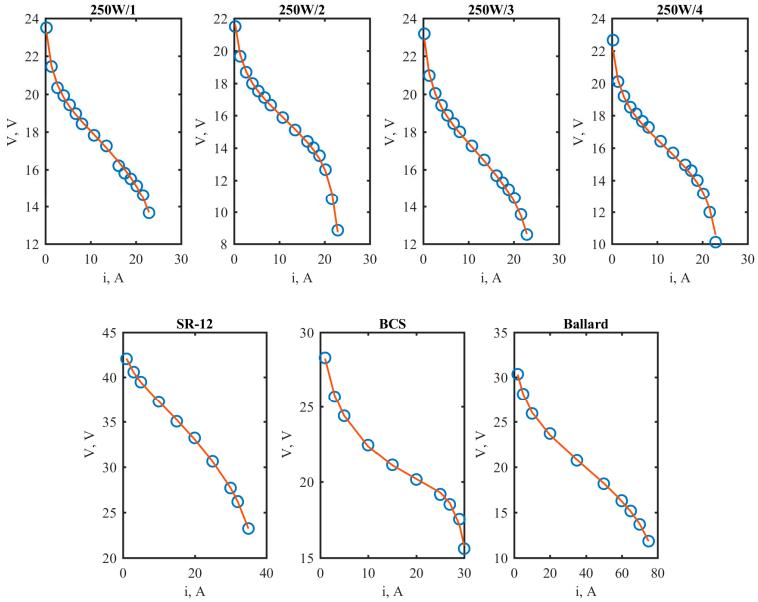

Figure 6. Polarization curves with the optimized model structure (solid line) and the experimental data (circles) interpreted from [9,17].

Table 2 shows that the optimized model structure led to better results than the model structure in [24] in terms of the *SSE* for the SR-12 and Ballard FCs. In the BCS case, [24] gives a better fit. For these three fuel cells, *SSE* values are very low, and both studies led to acceptable results. For the 250W FC, we had data on several operating points, and the optimized model structure results in significantly lower *SSE* than in [10]. In Ohenoja et al. [10], the best fit had an *SSE* value of 8.4854, whereas this model achieved an *SSE* of 1.6154. Yang et al. [15] reached even a lower *SSE* value of 1.1746 for the 250W FC. This was achieved by adding three more free parameters in the modeling and parameter fitting.

Table 2. Model performance for the studied fuel cells. *SSE*: sum of squared errors.

Fuel Cell	*SSE*			
	Case 1	**Ohenoja et al. [24]**	**Ohenoja et al. [10]**	**Case 2**
250W/1	0.2384			0.2739
250W/2	0.2782			0.7142
250W/3	0.2059			0.3107
250W/4	0.8929			0.0476
250W/all	1.6154		8.4854	1.3464
SR-12	0.0615	0.4475		0.5762
BCS	0.2148	0.1040		0.1427
Ballard	0.0640	0.0918		0.4825
Total *SSE*	1.96			2.55

The optimized model structure found for the FC polarization curve can be written as:

$$\hat{y} = a_0 + a_{1,2} f_1 \hat{f}_2 + a_3 f_3 + a_4 f_4 + a_{5,6} f_5 \div f_6 + a_7 f_7 \quad (4)$$

where:

$$f_1 = \frac{1}{C_{O2}}, f_2 = \frac{i}{i_{\lim}}, f_3 = 10^{\frac{i}{i\lim}}, f_4 = p_{H2}, f_5 = \sqrt{\frac{i}{i_{\lim}}}, f_6 = T, f_7 = 10^{-\frac{i}{i\lim}} \quad (5)$$

The linear regression coefficients $a_0 \ldots a_7$ are presented in the Supplementary Material. Equation (5) shows that the model structure that was found incorporates operating conditions (C_{O2}, p_{H2}, T). This is important in order to generalize the model predictions into different operating conditions. However, from the high *SSE* value for the 250W/4 polarization data, it is clear that this generalization ability is limited. Term i/i_{lim} is repeated several times in the optimized model. Indeed, i_{lim} has a strong effect on the polarization curve, as it determines the end point for the curve. In this exercise, it was assumed that the value for the i_{lim} is known and fixed throughout the operating conditions. Naturally, unknown i_{lim} values would require new model structure identification.

3.2. Case 2

As recognized in [7], the model structure search can also incorporate additional variables. Hence, the optimization is repeated with an altered set of input variables. In this case, the input variables were i, T, C_{O2}, p_{O2}, p_{H2}, L_{mem}, A, and i_{lim}. This way, the number of variable candidates remains constant. The model complexity is also kept at a comparable level by allowing up to seven terms in the resulting model. The resulting *SSE*s are presented in Table 2, and the optimized model structure in Equations (6) and (7):

$$\hat{y} = a_0 + a_{1,2,3} f_1 \div f_2 \times f_3 + a_4 f_4 + a_{5,6} f_5 \times f_6 + a_7 f_7 \quad (6)$$

where:

$$f_1 = 10^i, f_2 = T, f_3 = \ln(p_{O2}), f_4 = \ln(C_{O2}), f_5 = \ln(i), f_6 = \ln(L_{mem}), f_7 = i^2 \quad (7)$$

In this case, the model does not comprise $i_{lim.}$ This might result in a predicted polarization curve that has zero crossing outside the actual current range of the FC. Hence, predictions in high currents may not be reliable with this model structure. Additionally, the incorporation of the logarithmic transformation of i leads to a situation where the model cannot represent open-circuit voltage, as it has no solution when $i = 0$. However, such a shortage may also be found in the semi-empirical models, as discussed in [25]. The comparison of the *SSE* values between the two model structures shows that this model structure has a higher total error (2.55). A closer look at the *SSE* values shows that in Case 2, the prediction performance of the 250W FC was emphasized with a cost of the modeling performance of the three other fuel cells. This indicates a poor generalization ability for the model structure. Hence, the conclusion is that the variables set used in Case 1 is preferred over Case 2.

3.3. Case 3

In the third case, the effect of the model complexity on the model performance is studied. The structure search was performed with the number of allowable model terms varying between four and nine. The same variable candidates as in Case 1 were used. The resulted total *SSE*s (all data) and *SSE* for 250W FC are shown in Figure 7. As expected, the model performance increases as the number of allowable model terms increases. However, it is notable that only minor improvement is achieved after $n = 5$.

The results in Case 3 outperform the model fitting observed in [15], where a 10-parameter model structure had a *SSE* value of 1.1746 for the 250W FC. They focused on the high-current region, and proposed two new expressions for the high-current region in order to improve the curve-fitting properties of the semi-empirical model. In Figure 7, it is indicated that an even better model fitting for the 250W FC can be achieved with a nine-parameter model.

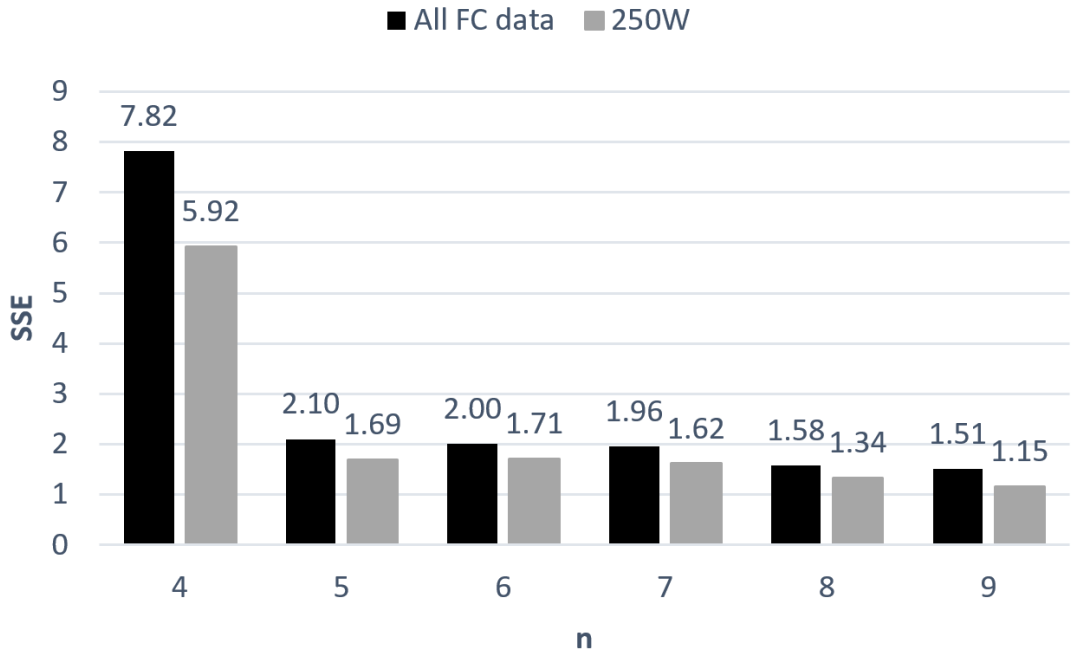

Figure 7. Objective function value with varying model complexity.

4. Discussion

The model structure found in this study (Case 1) provides very low *SSE* values with the same number of free parameters, and therefore with a comparable model complexity to the semi-empirical model structure used in [9,10,12,22,24]. Naturally, the remarkable difference in the observed *SSE* values can be partly explained with the constrained parameter values in the semi-empirical model. It was shown in [10] that the expanded search range leads to more accurate results. With the approach taken here, the optimization problem is unconstrained. It should also be noted that several authors have used the semi-empirical model structure, and have been able to find better *SSE* values than reported in [10] using different optimization algorithms. For example, Sun et al. [12] managed to reach a *SSE* value of 7.99 for the 250W fuel cell compared with 8.49 in [10]. However, the data sets are not exactly the same, although they were interpreted from the same original polarization curves. Therefore, the direct comparison of *SSE*s between different studies can be misleading.

In Case 2, the altered variable candidate list did not improve the model performance. An optimization case formulated with all of the possible variables, comprising ρ_m and the number of cells in an FC stack, for example, would be preferable. In addition, the structure identification could incorporate more than one nonlinear transformation in a series. Such alternations can be made with the approach presented, but require carefully made modifications to the optimization algorithm.

Based on the results in Case 3, the model structure search could be utilized to extend the work in [15]. It would be interesting to observe what kind of expression for the high-current region could be found with an evolutionary optimizer. However, in order to facilitate such a test, more data is required, as only a few data points in the polarization curve data that were utilized in this study are in this high-current region.

The approach taken in this study is fundamentally data-driven, and the link between the model parameter values and the physical phenomena that the mechanistic models hold is lost. However, the model structure established had (limited) generalization ability, and the model was linear with respect to its parameters. This feature can be beneficial in many FC system applications related to diagnostics, control, and large-scale simulations where easy model implementation or continuous adaptation is required. Naturally, an extension to dynamic models is required in such instances. The model structures that were identified in this study incorporated operating conditions, which can be linked to the mass and energy balances of an FC system. However, the model's ability to capture transient states requires further studies.

Typically, the data-driven methods use a rather vast amount of (measured) data and data pre-processing. In this exercise, the data were very limited. Although the model was efficiently fitted to four different fuel cell polarization curves, a more rigorous benchmark test with a rich data set is needed. Data originating from [9,17] provide only an example with the limited amount of data points. Benchmark data could be, for example, simulated via a rigorous model in different operating conditions with added noise and drift elements. Such data would allow efficient testing of the model performance.

5. Conclusions

A novel approach to find a generalizable FC polarization curve model structure utilizing only directly or indirectly measurable variables, known FC properties, and operating conditions was taken. The identification task was converted to an optimization problem and solved with binary coded genetic algorithms. The effect of model complexity on the model performance was investigated. The optimized model structure with comparable model complexity in comparison to the semi-empirical model structure utilized in a number of studies was found to outperform the semi-empirical model. A sufficient modeling result can also be achieved with lower model complexity. The results indicated a limited generalization ability with respect to different fuel cells and operating conditions, but proper benchmark data are required for more comprehensive tests in order to draw solid conclusions.

Supplementary Materials: The following are available online at http://www.mdpi.com/2073-431X/7/4/60/s1, Spreadsheet with fuel cell data, and regression coefficients for Case 1 and Case 2.

Author Contributions: Conceptualization, M.O.; Formal analysis, M.O.; Investigation, M.O.; Methodology, M.O. and A.S.; Software, M.O.; Supervision, K.L.; Validation, M.O.; Visualization, M.O.; Writing—original draft, M.O.; Writing—review & editing, A.S. and K.L.

Funding: This research received no external funding.

Conflicts of Interest: The authors declare no conflict of interest.

Appendix A

The auxiliary equations required to calculate the oxygen and hydrogen partial pressures and oxygen concentration are adopted from [9]. Equation (A1) solves the saturation pressure of water, Equations (A2) and (A3) solves the oxygen partial pressure in air fed FC and oxygen fed FC, respectively. Equation (A4) solves the oxygen concentration and Equation (A5) solves the hydrogen partial pressure.

$$\begin{aligned}\log_{10}(p^{sat}_{H2O}) = {} & -2.18 + 2.95 \cdot 10^{-2}(T - 273.15) \\ & -9.18 \cdot 10^{-5}(T - 273.15)^2 + 1.44 \cdot 10^{-7}(T - 273.15)^3\end{aligned} \tag{A1}$$

$$p_{O2} = \left(P_c - RH_c p_{H2O}^{sat}\right) \cdot \left[1 + \frac{0.79}{0.21} \cdot \exp\left(\frac{0.291(\frac{i}{A})}{T^{0.832}}\right)\right]^{-1} \tag{A2}$$

$$p_{O2} = \left(RH_c p_{H2O}^{sat}\right)\left\{\left[\exp\left(\frac{4.192(\frac{i}{A})}{T^{1.334}}\right)\left(\frac{RH_c p_{H2O}^{sat}}{P_c}\right)\right]^{-1} - 1\right\} \tag{A3}$$

$$C_{O2} = \frac{p_{O2}}{5.08 \cdot 10^6 \exp(-498/T)} \tag{A4}$$

$$p_{H2} = \frac{RH_a p_{H2O}^{sat}}{2}\left\{\left[\exp\left(\frac{1.635(\frac{i}{A})}{T^{1.334}}\right)\left(\frac{RH_a p_{H2O}^{sat}}{P_a}\right)\right]^{-1} - 1\right\} \tag{A5}$$

References

1. Sharaf, O.Z.; Orhan, M.F. An overview of fuel cell technology: Fundamentals and applications. *Renew. Sustain. Energy Rev.* **2014**, *32*, 810–853. [CrossRef]
2. Lee, J.H.; Lalk, T.R.; Appleby, A.J. Modeling electrochemical performance in large scale proton exchange membrane fuel cell stacks. *J. Power Sources* **1998**, *70*, 258–268. [CrossRef]
3. Mann, R.F.; Amphlett, J.C.; Hooper, M.A.I.; Jensen, H.M.; Peppley, B.A.; Roberge, P.R. Development and application of a generalised steady-state electrochemical model for a PEM fuel cell. *J. Power Sources* **2000**, *86*, 173–180. [CrossRef]
4. Pisani, L.; Murgia, G.; Valentini, M.; D'Aguanno, B. A new semi-empirical approach to performance curves of polymer electrolyte fuel cells. *J. Power Sources* **2002**, *108*, 192–203. [CrossRef]
5. Kulikovsky, A.A.; Wüster, T.; Egmen, A.; Stolten, D. Analytical and Numerical Analysis of PEM Fuel Cell Performance Curves. *J. Electrochem. Soc.* **2005**, *152*, A1290. [CrossRef]
6. Amphlett, J.C. Performance Modeling of the Ballard Mark IV Solid Polymer Electrolyte Fuel Cell. *J. Electrochem. Soc.* **1995**, *142*. [CrossRef]
7. Ohenoja, M.; Sorsa, A.; Leiviskä, K. Genetic Algorithms in Model Structure Identification for Fuel Cell Polarization Curve. In Proceedings of the 5th International Conference on Control, Decision and Information Technologies (CoDIT), Thessaloniki, Greece, 10–13 April 2018; pp. 539–544. [CrossRef]
8. Jourdani, M.; Mounir, H.; Marjani, A. Three-Dimensional PEM Fuel Cells Modeling using COMSOL Multiphysics. *Int. J. Multiphys.* **2017**, *11*. [CrossRef]
9. Mo, Z.-J.; Zhu, X.-J.; Wei, L.-Y.; Cao, G.-Y. Parameter optimization for a PEMFC model with a hybrid genetic algorithm. *Int. J. Energy Res.* **2006**, *30*, 585–597. [CrossRef]
10. Ohenoja, M.; Leiviskä, K. Validation of genetic algorithm results in a fuel cell model. *Int. J. Hydrogen Energy* **2010**, *35*, 12618–12625. [CrossRef]
11. Sorsa, A.; Koskenniemi, A.; Leiviskä, K. Differential evolution in parameter identification fuel cell as an example. In Proceedings of the 9th International Conference on Informatics in Control, Automation and Robotics (ICINCO 2012), Rome, Italy, 28–31 July 2012; Volume 1, pp. 40–49.
12. Sun, Z.; Wang, N.; Bi, Y.; Srinivasan, D. Parameter identification of PEMFC model based on hybrid adaptive differential evolution algorithm. *Energy* **2015**, *90*, 1334–1341. [CrossRef]
13. El-Fergany, A.A. Extracting optimal parameters of PEM fuel cells using Salp Swarm Optimizer. *Renew. Energy* **2018**, *119*, 641–648. [CrossRef]
14. Ali, M.; El-Hameed, M.A.; Farahat, M.A. Effective parameters' identification for polymer electrolyte membrane fuel cell models using grey wolf optimizer. *Renew. Energy* **2017**, *111*, 455–462. [CrossRef]
15. Yang, S.; Chellali, R.; Lu, X.; Li, L.; Bo, C. Modeling and optimization for proton exchange membrane fuel cell stack using aging and challenging P systems based optimization algorithm. *Energy* **2016**, *109*, 569–577. [CrossRef]
16. Chakraborty, U.K. Static and dynamic modeling of solid oxide fuel cell using genetic programming. *Energy* **2009**, *34*, 740–751. [CrossRef]
17. Xue, X.D.; Cheng, K.W.E.; Sutanto, D. Unified mathematical modelling of steady-state and dynamic voltage–current characteristics for PEM fuel cells. *Electrochim. Acta* **2006**, *52*, 1135–1144. [CrossRef]

18. Han, I.-S.; Chung, C.-B. Performance prediction and analysis of a PEM fuel cell operating on pure oxygen using data-driven models: A comparison of artificial neural network and support vector machine. *Int. J. Hydrogen Energy* **2016**, *41*, 10202–10211. [CrossRef]
19. Srinivasan, S.; Ticianelli, E.A.; Derouin, C.R.; Redondo, A. Advances in solid polymer electrolyte fuel cell technology with low platinum loading electrodes. *J. Power Sources* **1988**, *22*, 359–375. [CrossRef]
20. Kim, J. Modeling of Proton Exchange Membrane Fuel Cell Performance with an Empirical Equation. *J. Electrochem. Soc.* **1995**, *142*, 2670. [CrossRef]
21. Squadrito, G.; Maggio, G.; Passalacqua, E.; Lufrano, F.; Patti, A. An empirical equation for polymer electrolyte fuel cell (PEFC) behaviour. *J. Appl. Electrochem.* **1999**, *29*, 1449–1455. [CrossRef]
22. Correa, J.M.; Farret, F.A.; Canha, L.N.; Simoes, M.G. An electrochemical-based fuel-cell model suitable for electrical engineering automation approach. *IEEE Trans. Ind. Electron.* **2004**, *51*, 1103–1112. [CrossRef]
23. Michalewicz, Z. *Genetic Algorithms + Data Structures = Evolution Programs*; Springer: Berlin/Heidelberg, Germany, 1996; ISBN 978-3-662-03315-9.
24. Ohenoja, M.; Leiviska, K. Identification of electrochemical model parameters in PEM fuel cells. In Proceedings of the International Conference on Power Engineering, Energy and Electrical Drives, Lisbon, Portugal, 18–20 March 2009; pp. 363–368. [CrossRef]
25. Chakraborty, U.K. Reversible and Irreversible Potentials and an Inaccuracy in Popular Models in the Fuel Cell Literature. *Energies* **2018**, *11*, 1851. [CrossRef]